



1 **Monitoring European anthropogenic NO_x emissions from space**

2 Ronald J. van der A^{1*}, Jieying Ding^{1*}, Henk Eskes¹

3 ¹Royal Netherlands Meteorological Institute (KNMI), De Bilt, The Netherlands

4

5 *Corresponding authors: Ronald van der A (avander@knmi.nl), Jieying Ding (jieying.ding@knmi.nl)

6

7 **Abstract**

8 Since the launch of TROPOMI on the S5p satellite, NO₂ observations have become available
9 with a resolution of 3.5x5 km, which makes monitoring NO_x emissions possible at the scale of
10 city districts and industrial facilities. For Europe, emissions are reported on an annual basis for
11 country totals and large industrial facilities and made publicly available via the European
12 Environmental Agency (EEA). Satellite observations can provide independent and more timely
13 information on NO_x emissions. A new version of the inversion algorithm DECSO (Daily
14 Emissions Constraint by Satellite Observations) has been developed for deriving NO_x
15 emissions for Europe on a daily basis, averaged to monthly mean maps. The estimated
16 precision of these monthly emissions is about 25% for individual grid cells. These satellite-
17 derived emissions from DECSO have been compared to the officially reported European
18 emissions and spatial-temporal disaggregated emission inventories. The country total DECSO
19 NO_x emissions are close to the reported emissions and the emissions compiled by the
20 Copernicus Atmospheric Monitoring Service (CAMS). The comparison of the spatial
21 distributed NO_x emissions of DECSO and CAMS showed that the satellite-derived emissions
22 are often higher in cities, while similar for large power plants and slightly lower in rural areas.

23

24

25 **1. Introduction**

26 Nitrogen oxides (NO_x) concentrations play an important role in air quality, the nitrogen cycle,
27 and as precursor for climate gasses. Knowledge of NO_x emissions is also important for climate
28 studies (Shindell et al., 2005). Because of the importance of NO_x for air quality, both the
29 concentrations in air and emissions to air are regulated in Europe. Country total NO_x emissions



30 need to be reported by EU countries as part of the Convention for Long-Range Transboundary
31 Air Pollution (LRTAP, Pinterits et al., 2021) and the National Emission reductions Commitments
32 (NEC) Directive (NEC, 2023) of the European Union. More detailed emission inventories
33 including spatial distribution are compiled based on reported emissions, statistical
34 information (e.g. population density) and activity data. Examples of these inventories on a
35 global scale are the Emissions Database for Global Atmospheric Research (EDGAR, EC-JRC/PBL,
36 2011, Janssens-Maenhout et al., 2015) and the various global and regional emission
37 inventories developed in the context of the Copernicus Atmosphere Monitoring Service
38 (CAM5, Innes et al, 2019) of the EU Copernicus programme. These gridded emission
39 inventories are widely used for global atmospheric composition and regional air quality
40 modelling. The realism of the air quality model results depends largely on the accuracy of the
41 emission inventory (Thunis et al, 2021).

42 Since the availability of satellites capable of measuring NO_2 concentrations in the atmosphere,
43 methods have been developed to derive top-down emissions (Streets et al., 2013). These top-
44 down emissions have the major advantage that they are observation based. This fully
45 independent source of information provides the possibility to check reported emissions,
46 monitor rapid changes (e.g. due to the COVID-19 lockdowns) and has the potential of finding
47 unknown and unreported sources. Polar satellites with a global daily coverage within 1-3 days,
48 allow monitoring of changes in emissions on timescales of days to weeks. Satellites measure
49 total concentrations of trace gases, and the distinction of source sector type must be deduced
50 via the source location. A popular inversion technique for NO_x emissions is the divergence
51 method of Beirle et al. (2021, 2023), where the average flux is calculated in grid cells, assuming
52 local mass balance, to find the sources of the emissions. Although no model is needed in this
53 method, the required spatial derivations lead to noisy fields for daily overpasses, and it
54 provides useful emissions when averaged over a longer period. Furthermore, assumptions
55 must be made for the chemical lifetime, and simplifications lead to biases especially in
56 background emissions. A second class of methods is based on plume fitting (Fioletov et al.,
57 2022). This method can be applied to individual overpasses but needs well-defined plume
58 shapes which is not trivial for areas with multiple sources close together. Both these methods
59 simplify atmospheric transport as two-dimensional. For a full three-dimensional description
60 of transport and chemistry, a data assimilation or inverse modelling method is used to match



61 the model results and observations by adapting the emissions (Miyazaki et al., 2017, Fortems-
62 Cheiney et al., 2021). A typical application of satellite-derived emissions is the study of the
63 impact of recent events, like for example the effect of COVID regulations (Ding et al., 2020).
64 Top-down emissions are also used for the verification and support to improve current
65 emission inventories (Guevara et al., 2021; Crippa et al., 2023). Interesting aspects to study
66 more closely are the spatial distribution, seasonal time profiles and multi-annual trends of the
67 emissions.

68 In this study we present the latest version 6.3 of the Daily Emissions Constrained by Satellite
69 Observations DECSO (DECSO) inversion algorithm. The DECSO algorithm can be applied for
70 the operational monthly (or even daily) monitoring of emissions for any region worldwide
71 based on satellite observations of trace gases such as SO₂, NH₃ or NO₂. In this paper this new
72 DECSO version has been applied to NO₂ observations over Europe from the TROPOMI
73 instrument (Veeffkind et al., 2012) on board the Sentinel-5P satellite. The DECSO system is
74 efficient, requires only a single forward run of the chemistry-transport model and takes about
75 12 hours to process one month of data on a 30-core computer. Here, we will evaluate the
76 performance of DECSO on various spatial scales (from national to point sources) by
77 comparison with the various bottom-up emission inventories available for Europe. By
78 comparing satellite derived emissions with bottom-up emissions we gain insight in the
79 accuracy of both derived emission datasets.

80

81

82 **2. Methodology and data**

83

84 **2.1 DECSO: inversion of TROPOMI observations**

85 The inversion algorithm DECSO (Daily Emissions Constrained by Satellite Observations) has
86 been developed at KNMI for the purpose of deriving emissions for short-lived gases (Mijling
87 and van der A, 2012). DECSO is using a Kalman Filter implementation for assimilating
88 emissions. The emission forecast model is based on persistency from the analysis, while the
89 concentrations are calculated from the emissions by a chemical transfer model (CTM) and
90 compared to satellite observations. The sensitivity of concentrations to emissions is calculated



91 from multiple forward trajectories to account for the transport of the short-lived gas, but only
92 a single CTM forward run is needed. More detailed information on the method can be found
93 in Mijling and Van der A (2012), the validation is described in Ding et al. (2017a) and the
94 previous latest published version, i.e. DECSO v5.2, is described in Ding et al. (2020). Recent
95 developments of the algorithm to improve its resolution and quality have led to the release
96 of version 6.3. The most important updates are the use of a recent version of the chemical
97 transport model, improved TROPOMI observations and changes in the sensitivity matrix
98 calculations.

99 The chemical transport model in DECSO has been upgraded to the latest version of the
100 Eulerian regional off-line CTM CHIMERE v2020r3 (Menut et al., 2021). The implementation of
101 CHIMERE in DECSO was described in Ding et al. (2017b). In this study CHIMERE is combined
102 with the Copernicus Landcover 2019 data (Buchhorn et al., 2020) and HTAP v3-2018 for the
103 source sector split of the emissions. The meteorological input data for CHIMERE are the
104 operational ECMWF weather forecasts.

105 The sensitivity matrix, giving the relationship between emissions and concentrations is based
106 on trajectories calculated with a high temporal resolution (maximum 7.5 minutes). In the new
107 version the relationship is limited to a range of maximum 150 km to avoid effects of errors in
108 the trajectories over longer distances. The default settings of DECSO described here are for a
109 grid resolution of 0.2 degree. For higher grid resolutions, the settings for temporal resolution
110 and maximum trajectory distance are increased and reduced respectively.

111 The error parametrizations for the emission model and observations are based on the
112 Observation-minus-Forecast (OmF) and the Observation-minus-Analysis (OmA) statistics of
113 previous runs. The latest version of DECSO can also be applied to the simultaneously
114 optimisation of emissions of NO_x and NH₃ (Ding et al., 2024).

115 We are using the latest version 2.4 reprocessed and offline TROPOMI NO₂ observations (van
116 Geffen et al, 2022b) converted to super-observations as described in Ding et al. (2020). The
117 TROPOMI tropospheric column and averaging kernels have been recomputed by combining
118 the TM5-MP retrieval a-priori model output with the data in the level-2 file. This results in a
119 retrieved partial column from about 700 hPa (terrain following) to the surface. The
120 corresponding averaging kernels are rescaled using the 700hPa column air-mass factor and
121 are zero above the 700 hPa level. This procedure removes NO₂ in the free troposphere caused



122 by, for example, lightning or long-range transport, which is known to be a significant source of
123 error (Douros et al., 2023).

124 Superobservations (Sekiya et al., 2022) are constructed as the area-weighted mean of cloud-
125 free (qa value > 0.75) TROPOMI observations over the CHIMERE model grid cells. For a grid of
126 0.2x0.2 degree a superobservation contains about 10 to 15 TROPOMI NO₂ observations. The
127 use of superobservations improves the signal-to-noise ratio and it reduces the calculation time
128 of DECSO. On the other hand, the sampling of transported NO₂ from the observations
129 calculated back to the source on the emission grid, based on superobservations, will slightly
130 spread out the derived emissions and reduce their spatial resolution compared to using
131 individual observations. The chosen size of the superobservation grid of 0.2x0.2 degree is
132 therefore a compromise between noise, calculation speed and spatial resolution. Knowing
133 that the smoothing of emissions after averaging can be imagined as a distribution by a pyramid
134 shape weighting function around a point source, a deconvolution is possible for isolated
135 emission sources with a known location. The current version of DECSO makes use of the
136 superobservations software as also used in Sekiya et al. 2022. The software has been further
137 developed focusing on a realistic description of the superobservation uncertainty (Rijsdijk et
138 al, 2024) and this new software will be used in future DECSO studies

139 In a post-processing step, the total monthly NO_x emissions are split into anthropogenic and
140 biogenic contributions. This is based on the assumption that biogenic emissions show a strong
141 seasonal cycle with low emissions in winter, while the anthropogenic emissions are more
142 constant over the year. This splitting method is detailed described in detail in Lin et al. (2023).

143 For the monthly emissions also the precision of the emission in each grid cell has been
144 calculated. Each daily NO_x emission per grid cell derived by DECSO is accompanied by a
145 standard deviation calculated according the Kalman Filter equations. As the starting point of
146 each daily step in the calculation by DECSO is the emissions of the previous day, the resulting
147 emissions will show an autocorrelation in their errors. For each grid cell the autocorrelation
148 function ρ_k (for time lag k) has been calculated for each month. We see typically that the
149 autocorrelation effects in the errors have disappeared completely after about 1 week.

150 When calculating the variance of the monthly mean values, we must take this autocorrelation
151 function into account. The variance S of the monthly mean NO_x emissions per grid cell is
152 calculated following Bayley and Hammersley (1946) or Box et al. (2008) as



153

154

$$S = \frac{\sigma^2}{n} \left[1 + 2 \sum_{k=1}^{n-1} \left(1 - \frac{k}{n} \right) \rho_k \right],$$

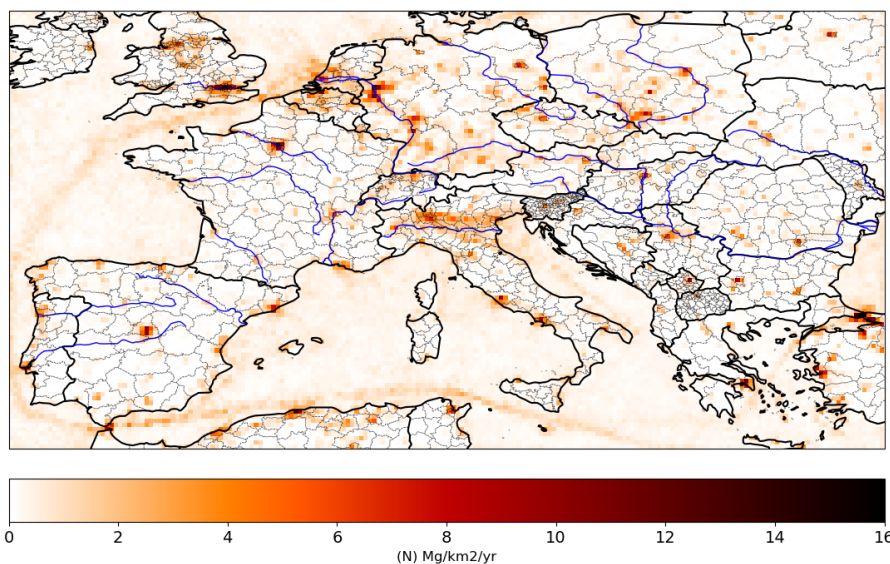
155

156 where σ is the mean standard deviation of the emissions over the month and n is the number
157 of days in the month. We assume here that σ is not varying a lot over the month. This precision
158 σ is calculated in the Kalman equations of the inverse modelling and it depends on the
159 precision of the TROPOMI NO₂ superobservations. The precision depends on the location and
160 emission magnitude, but on average the precision is estimated as 8% for annual emissions,
161 25% for monthly emissions and between 10 and 60 % for the daily emissions.

162

163 In this study we will focus only on NO_x emissions. Although DECSO has been applied to many
164 regions in the world, in this study we will show results for a domain over Europe (35°-55°N, 10°
165 W-30°E) and for 0.2 degree spatial resolution. The temporal resolution of our inversion is daily,
166 usually averaged to monthly or yearly mean values, for the period of 2019 to 2022. Figure 1
167 show the average annual emissions for 2019 as derived with DECSO version 6.3.

168



169

170

Figure 1 The annual-averaged anthropogenic NO_x emissions for 2019 derived from TROPOMI NO₂ observations using the DECSO algorithm.

171



172

173

174 **2.2 Databases for validation**

175 For comparison of the emission results in Europe we will use several inventories, all based on
176 official emissions reported to the European Environmental Agency (EEA). The first one is the
177 inventory of national emissions per source category reported under the National Emission
178 reductions Commitments (NEC) Directive of the European Union. Another similar inventory is
179 the Emission inventory reported under the Convention on Long-range Transboundary Air
180 Pollution (LRTAP), which give the country totals of emissions in various source categories. The
181 last one we will use is the European Pollutant Release and Transfer Register (E-PRTR; EPTR, 2012),
182 which is a database of the individual emissions of the biggest industrial facilities (above
183 0.1Mg/year) in Europe. From here on we will call those databases simply NEC, LRTAP and E-
184 PRTR. Besides comparison with these officially reported emissions, we will also compare our
185 emissions to the regional anthropogenic emission inventory CAMS-REG-ANT v5.1 for air
186 quality in Europe (Kuenen et al., 2022) developed for the Copernicus Atmospheric Monitoring
187 Service (CAMS), hereafter called CAMS-REG. For these CAMS-REG emissions we use the total
188 emissions regridded from $0.1^\circ \times 0.05^\circ$ to $0.2^\circ \times 0.2^\circ$ and exclude the agricultural emissions,
189 which are also excluded in DECSO. Temporal profiles are also derived in CAMS, which allow us
190 to compare timeseries. We will use the Copernicus Atmosphere Monitoring Service TEMPORal
191 profiles (CAMS-GLOB-TEMPO, Guevara et al., 2021,2023) for comparison of monthly
192 variations in anthropogenic NO_x emissions. The global emission data version 5.3, called CAMS-
193 GLOB-TEMPO, on a resolution of $0.1^\circ \times 0.1^\circ$ has been regridded to $0.2^\circ \times 0.2^\circ$ resolution and is
194 hereafter referred to as CAMS-TEMPO.

195

196 **3. Evaluation of the satellite derived emissions**

197

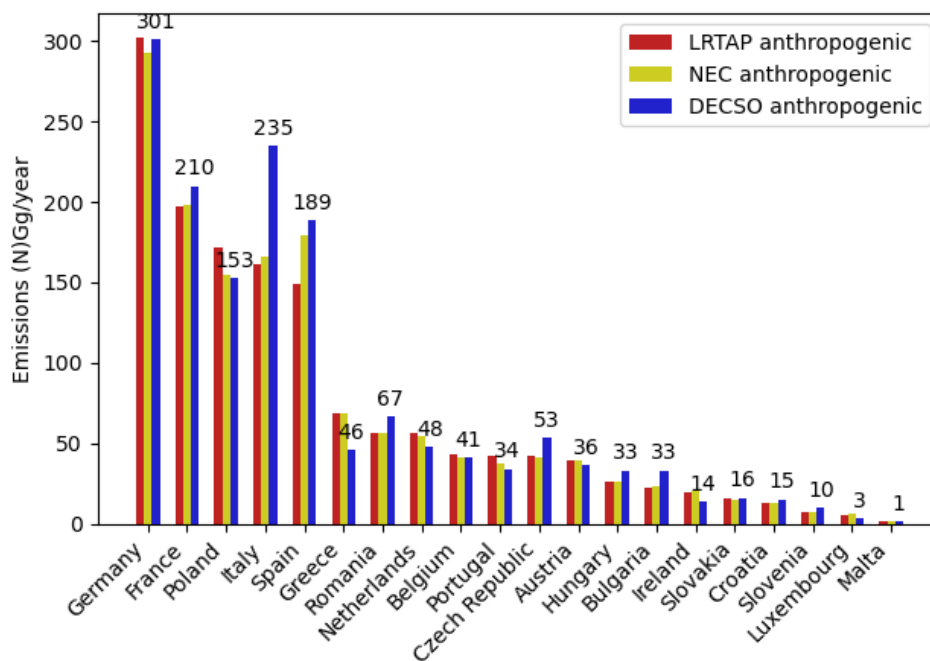
198 **3.1 Country scale intercomparison**

199 The NO_x emissions derived with DECSO have been summed over the countries (weighted by
200 the land-fraction per grid cell) in our domain and compared to the registered total emissions
201 in NEC and LRTAP. Note that for the national total emissions the spatial resolution or spatial



202 smoothing of the derived emissions play hardly any role. In total 21 countries are completely
203 covered by our geographical domain and have reported their emissions. The total
204 anthropogenic emissions (excluding agricultural emissions) for all these 21 countries are 1.44
205 Tg/year according both LRTAP and NEC. The total calculated anthropogenic emissions by
206 DECSO are 1.54 Tg/year, about 7% higher than the reported emissions. The total
207 anthropogenic emissions of CAMS-REG (excluding agricultural emissions) for the same region
208 are 1.54 Tg/year, in agreement with DECSO. Note that the total soil emissions derived by
209 DECSO are 0.78 Tg/yr for the same region, but this number cannot be compared because soil
210 emissions in LRTAP and NEC are only given for the agricultural sector and not for forestry. The
211 anthropogenic country totals are shown in Figure 2. In general, we see a good agreement per
212 country except for Italy, which has much lower reported emissions. Greece, on the other hand,
213 has higher registered emissions, but the mismatch might be related to the difficult counting
214 over the Greek islands, since these emissions are weighted by the land fraction in the grid cell
215 of DECSO to exclude maritime emissions in our counting. Note that Ireland is only partly in our
216 geographical domain and has therefore lower emissions according to DECSO. Besides the
217 comparison on a national level also on a provincial scale good agreement is found, as has been
218 shown for Catalonia by Mijling et al. (2023).

219



220

221 **Figure 2** Country totals of anthropogenic NOx emissions (in (N)Gg/year) in the year
 222 2019 according to databases LRTAP and NEC and the DECSO calculations.

223

224

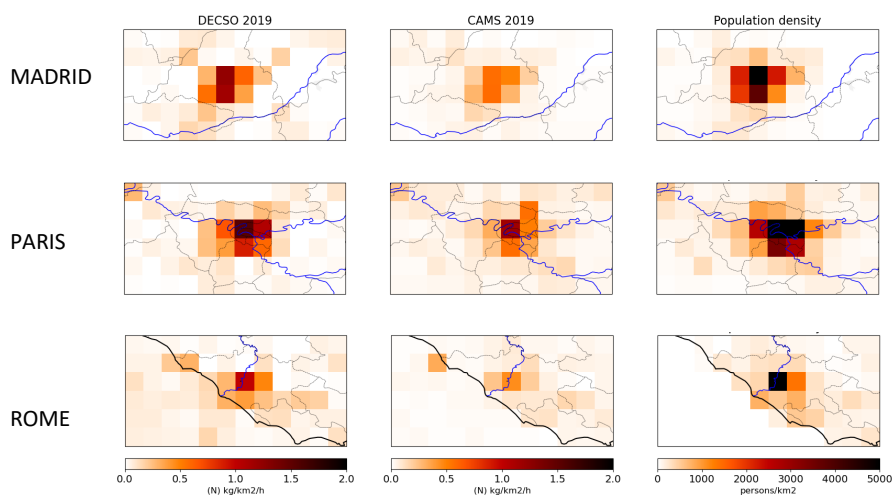
225 **3.2 City scale**

226 With our current spatial resolution of 0.2x0.2 degree, we observe emissions per city district
 227 for mega cities, but the geographical distribution can be slightly blurred by the 0.2 degree
 228 resolution of the TROPOMI superobservations. Figure 3 shows the spatial distribution of the
 229 annual emissions of DECSO and CAMS-REG for three of the largest megacities in Europe:
 230 Madrid, Paris, and Rome. Although DECSO show similar emissions for the country totals, we
 231 see that for megacities DECSO estimates higher emissions in the city center, and more
 232 activities are seen in the region surrounding the city, as compared to the CAMS emissions. The
 233 industrial complexes at Rouen located north-west of Paris, and at the port of Civitavecchia
 234 located west of Rome are similar in DECSO compared to CAMS-REG. The area of Rouen used
 235 to have an active oil refinery, but in recent years the industrial emissions are about 0.11
 236 (N)kg/km²/h according to the E-PRTR database, which compares well to CAMS-REG and



237 DECSO. The spatial extent of high emissions in the Rome area is smaller in CAMS, which follows
238 more the population density. However, the densely populated center of Rome is surrounded
239 by a busy ring road with a 20 km radius and a lot of commercial activities around the city,
240 which are not reflected in the population density map. The two powerplants at Civitavecchia
241 have reported emissions according to the E-PRTR database, which are equivalent to about
242 0.17 (N)kg/km²/h per grid cell, which is closer to the DECSO derived emissions. Although this
243 study focuses mainly on the land emissions, we see in the map for Rome, that the maritime
244 emissions of CAMS and DECSO disagree a lot, and this is a topic for further studies.

245



246 **Figure 3** Zoom-in plots for 3 megacities in Europe to illustrate the differences in
247 distribution of emissions of DECSO (first column), CAMS-REG (second column) and the
248 population density (third column) per km².

249

250 Figure S1 in the supplement is an example of a timeseries for city emissions, in this case for
251 the city of Paris. The time series show 3 low emission periods: in Nov. 2019 (reason unknown),
252 in April 2020 when COVID hits Europe, and in the winter of 2020-2021 when strict COVID
253 regulations were in place. After the recovery from COVID we see that emissions grow again in
254 2022 to the level of pre-COVID.

255



256

257 **3.3 Intercomparison for large point sources**

258 To evaluate the performance of monitoring emissions from large point sources (LPS), we
259 compare the DECSO emissions with emissions registered in the E-PRTR data base. The isolated
260 LPS in Europe we selected are all large power plants close to lignite mines. Emissions from
261 DECSO are slightly spread to adjacent grid cells because the spatial resolution of the emission
262 field is less than the sampling of the grid cells as discussed in Sect. 2. To correct for this, we
263 can deconvolute the emissions around the isolated point source, but here we choose to sum
264 the anthropogenic emissions in the 3x3 grid cells including and around the point source to
265 make sure all emissions are accounted for. For the four cases discussed below, no significant
266 other sources exist in these 3x3 grid cell boxes, and biogenic emissions are excluded. The rural
267 anthropogenic emissions in such an area of 3x3 grid cells in Europe we estimate as about 0.13
268 (N)Gg/year by averaging the emissions of several similar rural 3x3 regions in Europe. We did
269 not correct for this background signal.

270 The first case is that of the Maritsa Iztok facility in Bulgaria located next to an open coal mine.
271 There is no big city or any other industrial facility in the neighborhood, except for the three
272 big power plants of the Maritsa Iztok facility. Figure 4 shows the monthly averaged emissions
273 calculated by the DECSO algorithm, the CAMS-TEMPO inventory, and the annual emissions
274 from the E-PRTR database for the Maritsa facility. For a fair comparison we selected for CAMS-
275 TEMPO also the same 3x3 grid cells around the LPS. For the period 2019-2022 the annual
276 emissions are given in Table 1 according to DECSO, CAMS-TEMPO and E-PRTR. The difference
277 in annual emissions between DECSO, CAMS-TEMPO and E-PRTR of the Maritsa facility are
278 relatively small, although DECSO is the highest. The CAMS-TEMPO emissions show a negative
279 trend, which is not visible in DECSO that shows the highest emissions for 2022. Unfortunately,
280 no E-PRTR data for 2022 is yet publicly available.

281 The second power plant is the Bełchatów power plant with its capacity of 5,053 MW, the
282 biggest power plant of Europe. It is also one of the most polluting power plants in the world
283 and gets its fuel from the adjacent lignite coal mine of Bełchatów (Guevara et al., 2023). For
284 the year 2020 no emission values are reported in the current E-PRTR database. For the years
285 2019 and 2021 DECSO observes high emissions of about 5.5 Gg per year, but this is lower than
286 the reported value of more than 7 Gg per year. CAMS-TEMPO also shows lower emissions with

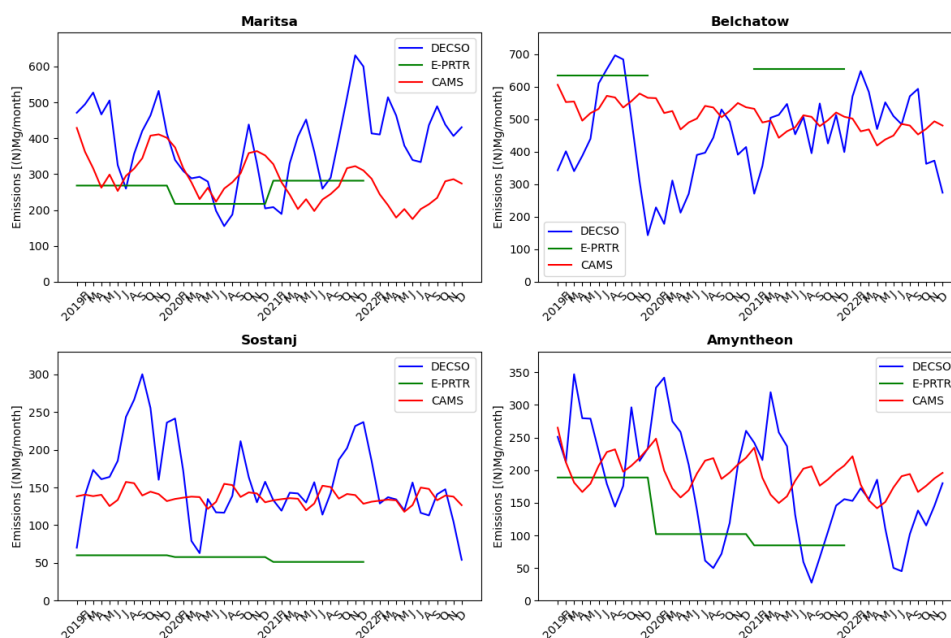


287 a negative trend. Godłowska et al. (2023) showed the stack measurements of this power plant
288 in their Figure 7, which also are in general lower than the E-PRTR values.

289 The next selected isolated power plant is the Šoštanj lignite power plant in the Velenje basin
290 in a mountainous area of Slovenia. It is responsible for one third of the electricity need of
291 Slovenia (Boznar et al., 2012). For this LPS both CAMS-TEMPO and DECSO show more than
292 two times higher emissions than E-PRTR, which is too large to be explained by the small cities
293 or other small sources located in the neighborhood.

294 The last case is that of the power plants of the Ptolemais-Amyntheon and Florina coal basins
295 in West Macedonia, Greece, which were also studied by Skoulidou et al. (2021). There are 5
296 power plants associated with and located at this basin, but only three are still active: Agios
297 Dimitrios (1595 MW), Kardias (1200 MW), and Amyntheon (600 MW) (Kostakis, 2009). For
298 2021 no data was reported for Amyntheon in the E-PRTR database. The reported values of the
299 E-PRTR database match those of CAMS-TEMPO and DECSO quite well, except for the year 2020
300 that marks the start of a decrease in emissions in this region. The decreasing trend can be
301 seen in all three emissions time lines, but is strongest in the E-PRTR time series. Most notable
302 in the Figure is the strong seasonal cycle in DECSO NO_x emissions for the Greek power plants
303 with the lowest emissions in summer time. This can be related to the availability of more
304 sustainable energy sources in the summer months.

305



306

307 **Figure 4** Timeseries of the NO_x emissions of the selected LPS in Europe as estimated by
308 DECSO (blue line), E-PRTR (green line) and CAMS-TEMPO (red line).

309

310 From this comparison for several large LPS in Europe, we see that CAMS-TEMPO and DECSO
311 are often larger than the reported emissions in E-PRTR. The annual values of CAMS-TEMPO
312 and DECSO are often in reasonable agreement (within 20%), but the variability of DECSO is
313 much higher. The CAMS-TEMPO emissions in the period 2019 to 2022 show for most studied
314 LPS a constant negative trend, which was generally not detected in DECSO. Without additional
315 information it is difficult to draw any conclusions on the performance for LPS, but DECSO
316 supplies additional information on these industrial facilities in Europe and the largest
317 discrepancies may be caused by strong diurnal variability (while TROPOMI observes at about
318 13:30) and will be interesting for further investigation.

319 In all cases we see lower emissions in 2020 during the COVID-19 pandemic. In this period the
320 demand of energy was lower and while renewable energy output remained similar, the energy
321 from lignite-based power plants was in relatively less demand (Quitow et al., 2021).

322



323 **Table 1** Annual NO_x emissions (N)Gg/year of the four lignite power plants.

Facility	2019			2020			2021			2022		
	CAMS	DECSO	E-PRTR	CAMS	DECSO	E-PRTR	CAMS	DECSO	E-PRTR	CAMS	DECSO	E-PRTR
Maritsa	4.1	5.2	3.2	3.6	3.3	2.6	3.2	4.6	3.4	2.8	5.0	-
Belchatow	6.6	5.5	7.6	6.3	4.3	-	5.9	5.4	7.9	5.6	6.0	-
Sostanj	1.7	2.4	0.69	1.7	1.7	0.66	1.6	1.9	0.62	1.5	1.3	-
Amyntheon	2.5	2.8	2.3	2.4	2.3	1.2	2.3	2.0	1.0	1.6	1.3	-

324

325

326 **4. Discussion**

327 We presented the latest version of the DECSO algorithm, version 6.3. Updates has been made
 328 for the superobservations, the chemical transport model, the sensitivity matrix and the error
 329 parametrization. The new version includes also an error estimate for the monthly NO_x
 330 emission data taking into account the autocorrelation in time. The new DECSO version has
 331 been applied to the domain of Europe and show more spatial details than before as a result
 332 of the higher resolution of TROPOMI observations compared to earlier satellite observations.

333 In the comparison with CAMS-REG over Europe (where emissions are usually well-known) the
 334 deviations are small (within 10%) when looking at country scale. For point sources the spread
 335 in the differences is much higher, but no systematic effect is yet found. For cities DECSO show
 336 higher emissions, while CAMS is higher for rural regions. On a European scale the biggest
 337 difference between CAMS-REG and DECSO was found for the region West of Belgrade in
 338 Serbia, where the Nicola Tesla power plants are located. While these show up as a strong
 339 emission source close to Belgrade in both the DECSO emissions and the E-PRTR database, they
 340 are not included or mislocated in the CAMS emissions. This is a prominent example that
 341 demonstrates the value of monitoring emissions with satellite observations.

342 The precision of the derived emissions by DECSO are given for each grid cell in the data files.
 343 In general, we can say that the precision of NO_x emissions given per grid cell (0.2x0.2 degree)
 344 is about 8% for annual emissions, 25% for monthly emissions and between 10 and 60 % for



345 the daily emissions. When averaging over a larger domain the precision will of course become
346 higher by the square root of the number of grid cells.

347 The comparison between CAMS and DECSO showed that DECSO is very similar on average.
348 While compared to the reported emissions in NEC or LRTAP, DECSO is 7 % higher. Validation of
349 the TROPOMI NO₂ observations showed that, when using averaging kernels, the bias of the
350 tropospheric column is estimated as -8% on average by comparison with MAX-DOAS
351 observations (Keppens and Lambert, 2023). This bias of -8% should result in lower emissions
352 by DECSO and the deviation between DECSO and other inventories would be higher in reality.
353 Keppens and Lambert further report that for polluted regions the mean bias of the TROPOMI
354 NO₂ observations is stronger, about -29%, while for clean areas the median bias is positive and
355 about +13% (when using averaging kernels). This would be contradictory to our findings over
356 cities, where DECSO shows higher emissions than CAMS-REG. Another potential cause of
357 biases in our emissions is the CHIMERE model. More research is needed for a better
358 understanding of the validation results of TROPOMI observations, CHIMERE performance, and
359 the comparisons between DECSO and CAMS.

360 This study shows the potential of DECSO for operational emission monitoring for Europe. The
361 monitoring of LPS only gives mainly clear results for isolated sources, thus an easy
362 improvement can be gained by providing the emissions on a higher resolution. DECSO has
363 already demonstrated its performance on a 0.1°x0.1° for the Yangtze River Delta (Zhang et al.,
364 2023), West Siberia (van der A et al., 2020), Spain and the Netherland.

365 In this study the focus was on Europe, but in other regions of the world emissions might be
366 less well-known. For these regions DECSO can or has been applied since we have global
367 satellite observations. Recently we have applied DECSO to areas in Africa, where several mines
368 with high NO_x emissions were found that were unreported in bottom-up emission inventories
369 like EDGAR or CAMS. This shows the possibilities also for application of DECSO in the Global
370 South.

371

372 **Data availability**

373 The TROPOMI NO₂ data version 2.4 are available via the Copernicus website

374 <https://dataspace.copernicus.eu/> and via the TEMIS website

375 <https://www.temis.nl/airpollution/no2.php>. The NO_x emissions of DECSO v6.3 are available on the



376 GlobEmission website: https://www.temis.nl/emissions/region_europe/datapage_nox.php. The
377 European emissions data sets for countries NEC, LRTAP and large facilities E-PRTR are available on the
378 website <https://www.eea.europa.eu/en/analysis> of the EEA. The CAMS databases CAMS-REG-ANT
379 v5.1 and CAMS-GLOB-TEMPO v3.1 are available on the ECCAD website on respectively
380 <https://permalink.aeris-data.fr/CAMS-REG-ANT> and <https://permalink.aeris-data.fr/CAMS-GLOB->
381 TEMPO.

382

383 **Author contributions**

384 RA and JD made the improvements to DECSO, HE developed the superobservation code. RA
385 did the processing, visualisations and main writing. JD and HE reviewed and edited the
386 manuscript.

387

388 **Competing interests**

389 The authors declare that they have no conflict of interest.

390

391 **Acknowledgments**

392 This research was part of the Sentinel EO-based Emission and Deposition Service (SEEDS,
393 Grant ID 101004318) project that has received funding from the European Union's Horizon
394 2020 research and innovation programme. Sentinel-5 Precursor is a European Space Agency
395 (ESA) mission on behalf of the European Commission. The TROPOMI payload is a joint
396 development by ESA and the Netherlands Space Office. The Sentinel-5 Precursor ground
397 segment development has been funded by ESA and with national contributions from the
398 Netherlands, Germany, and Belgium. This work contains modified Copernicus Sentinel-5P
399 TROPOMI data (2018–2023), processed locally at KNMI.

400

401

402

403 **References**



- 404 Bayley, G. V., & Hammersley, J. M. (1946). The “Effective” Number of Independent Observations in an
405 Autocorrelated Time Series. Supplement to the Journal of the Royal Statistical Society, 8(2), 184-197,
406 <https://doi.org/10.2307/2983560>
- 407 Beirle, S., Borger, C., Dörner, S., Eskes, H., Kumar, V., de Laat, A., and Wagner, T.: Catalog of NO_x emissions from
408 point sources as derived from the divergence of the NO₂ flux for TROPOMI, Earth Syst. Sci. Data, 13, 2995-3012,
409 <https://doi.org/10.5194/essd-13-2995-2021>, 2021.
- 410 Beirle, S., Borger, C., Jost, A., and Wagner, T.: Improved catalog of NO_x point source emissions (version 2), Earth
411 Syst. Sci. Data, 15, 3051–3073, <https://doi.org/10.5194/essd-15-3051-2023>, 2023.
- 412 Box, Jenkins, Reinsel, Time Series Analysis: Forecasting and Control, 4th Ed. Wiley (2008), ISBN 978-0-470-
413 27284-8, p.30.
- 414 Božnar, M.Z., Mlakar, P., Grašič, B. and Tinarelli, G. (2012), Environmental impact assessment of a new thermal
415 power plant Šoštanj Block 6 in highly complex terrain, Int. J. Environment and Pollution, Vol. 48, Nos. 1/2/3/4,
416 pp.136–144.
- 417 Buchhorn, M. ; Smets, B. ; Bertels, L. ; De Roo, B. ; Lesiv, M. ; Tsendbazar, N. - E. ; Herold, M. ; Fritz, S,
418 Copernicus Global Land Service: Land Cover 100m: collection 3: epoch 2019: Globe, 2020, DOI:
419 10.5281/zenodo.3939050
- 420 Crippa, M., Guizzardi, D., Butler, T., Keating, T., Wu, R., Kaminski, J., Kuenen, J., Kurokawa, J., Chatani, S.,
421 Morikawa, T., Pouliot, G., Racine, J., Moran, M. D., Klimont, Z., Manseau, P. M., Mashayekhi, R., Henderson, B.
422 H., Smith, S. J., Suchyta, H., . . . Foley, K. (2023). The HTAP_v3 emission mosaic: merging regional and global
423 monthly emissions (2000–2018) to support air quality modelling and policies. Earth Syst. Sci. Data, 15(6), 2667-
424 2694. <https://doi.org/10.5194/essd-15-2667-2023>
- 425 Ding, J., Miyazaki, K., van der A, R.J., Mijling, B., Kurokawa, J., Cho, S., Janssens-Maenhout, G., Zhang, Q., Liu, F.,
426 and Levelt, P.F., Intercomparison of NO_x emission inventories over East Asia, Atm. Chem. Phys., 2017a, 17,
427 10125-10141, doi.org/10.5194/acp-17-10125-2017
- 428 Ding, J., R.J. van der A, B. Mijling and P.F. Levelt, Space-based NO_x emission estimates over remote regions
429 improved in DECSO, Atmospheric Measurement Techniques, 2017b, 10, 925-938, [doi:10.5194/amt-10-925-](https://doi.org/10.5194/amt-10-925-2017)
430 2017.
- 431 Ding, J., van der A, R. J., Eskes, H. J., Mijling, B., Stavrakou, T., van Geffen, J. H. G. M., Veefkind, J.P., NO_x
432 emissions reduction and rebound in China due to the COVID-19 crisis, Geophysical Research Letters, 46,
433 e2020GL089912. <https://doi.org/10.1029/2020GL089912>, 2020.
- 434 Ding et al., NH₃ emissions from CrIS observations using DECSO, in preparation, 2024
- 435 Douros, J., Eskes, H., van Geffen, J., Boersma, K. F., Compernelle, S., Pinardi, G., Blechschmidt, A.-M., Peuch, V.-
436 H., Colette, A., and Veefkind, P.: Comparing Sentinel-5P TROPOMI NO₂ column observations with the CAMS



- 437 regional air quality ensemble, *Geosci. Model Dev.*, 16, 509–534, <https://doi.org/10.5194/gmd-16-509-2023>,
438 2023.
- 439 EC-JRC/PBL, European Commission, Joint Research Centre (JRC)/Netherlands Environmental Assessment
440 Agency (PBL): Emission Database for Global Atmospheric Research (EDGAR), release EDGAR version 4.2,
441 available at: <http://edgar.jrc.ec.europa.eu/overview.php?v=42>, 2011.
- 442 EPRT: European Pollutant Transfer Register, database version v4.2, available at: <http://prtr.ec.europa.eu/> (last
443 access: 5 September 2023), 2012.
- 444 Fioletov, V., McLinden, C. A., Griffin, D., Krotkov, N., Liu, F., and Eskes, H.: Quantifying urban, industrial, and
445 background changes in NO₂ during the COVID-19 lockdown period based on TROPOMI satellite observations,
446 *Atmos. Chem. Phys.*, 22, 4201–4236, <https://doi.org/10.5194/acp-22-4201-2022>, 2022.
- 447 Fortems-Cheiney, A., Broquet, G., Pison, I., Saunois, M., Potier, E., Berchet, A., et al. (2021). Analysis of the
448 anthropogenic and biogenic NO_x emissions over 2008–2017: Assessment of the trends in the 30 most
449 populated urban areas in Europe. *Geophysical Research Letters*, 48, e2020GL092206.
450 <https://doi.org/10.1029/2020GL092206>
- 451 Guevara, M., Jorba, O., Tena, C., Denier van der Gon, H., Kuenen, J., Elguindi, N., Darras, S., Granier, C., and
452 Pérez García-Pando, C.: Copernicus Atmosphere Monitoring Service TEMPOral profiles (CAM5-TEMPO): global
453 and European emission temporal profile maps for atmospheric chemistry modelling, *Earth Syst. Sci. Data*, 13,
454 367–404, <https://doi.org/10.5194/essd-13-367-2021>, 2021.
- 455 Guevara, M., Enciso, S., Tena, C., Jorba, O., Dellaert, S., Denier van der Gon, H., and Pérez García-Pando, C.: A
456 global catalogue of CO₂ emissions and co-emitted species from power plants at a very high spatial and
457 temporal resolution, *Earth Syst. Sci. Data Discuss.* [preprint], <https://doi.org/10.5194/essd-2023-95>, in review,
458 2023.
- 459 Godfowska, J., M. J. Hajto, B. Lapeta, K. Kaszowski, The attempt to estimate annual variability of NO_x emission
460 in Poland using Sentinel-5P/TROPOMI data, *Atmospheric Environment*, Vol. 294, 2023, 119482,
461 <https://doi.org/10.1016/j.atmosenv.2022.119482>.
- 462 Inness, A., Ades, M., Agustí-Panareda, A., Barré, J., Benedictow, A., Blechschmidt, A.-M., Dominguez, J. J.,
463 Engelen, R., Eskes, H., Flemming, J., Huijnen, V., Jones, L., Kipling, Z., Massart, S., Parrington, M., Peuch, V.-H.,
464 Razinger, M., Remy, S., Schulz, M., and Suttie, M.: The CAM5 reanalysis of atmospheric composition, *Atmos.*
465 *Chem. Phys.*, 19, 3515–3556, <https://doi.org/10.5194/acp-19-3515-2019>, 2019.
- 466 Janssens-Maenhout, G., Crippa, M., Guizzardi, D., Dentener, F., Muntean, M., Pouliot, G., Keating, T., Zhang, Q.,
467 Kurokawa, J., Wankmüller, R., Denier van der Gon, H., Kuenen, J. J. P., Klimont, Z., Frost, G., Darras, S., Koffi, B.,
468 and Li, M. HTAP_v2.2: a mosaic of regional and global emission grid maps for 2008 and 2010 to study
469 hemispheric transport of air pollution *Atmos. Chem. Phys.* 15, 11411–11432, 2015



- 470 Keppens, A. and Lambert, J.-C. (editors), Quarterly Validation Report of the Copernicus Sentinel-5 Precursor
471 Operational Data Products #19: April 2018 – May 2023, S5P-MPC-IASB-ROCVR-19.01.00-20230703, version
472 19.01.00 3 July 2023, (available at <https://mpc-vdaf.tropomi.eu/>).
- 473 Kostakis, G., Characterization of the fly ashes from the lignite burning power plants of northern Greece based
474 on their quantitative mineralogical composition, *Journal of Hazardous Materials*, Vol. 166, 2009, Pages 972-
475 977, <https://doi.org/10.1016/j.jhazmat.2008.12.007>.
- 476 Kuenen, J., Dellaert, S., Visschedijk, A., Jalkanen, J.-P., Super, I., and Denier van der Gon, H.: CAMS-REG-v4: a
477 state-of-the-art high-resolution European emission inventory for air quality modelling, *Earth Syst. Sci. Data*, 14,
478 491–515, <https://doi.org/10.5194/essd-14-491-2022>, 2022.
- 479 Lin, X., R. J. van der A, J. de Laat, V. Huijnen, B. Mijling, J. Ding, H. Eskes, J. Douros, M. Liu, X. Zhang, Z. Liu,
480 European soil NOx emissions derived from satellite NO2 observations. *ESS Open Archive* . December 10, 2023.
- 481 Menut, L., Bessagnet, B., Khvorostyanov, D., Beekmann, M., Blond, N., Colette, A., Coll, I., Curci, G., Foret, G.,
482 Hodzic, A., Mailler, S., Meleux, F., Monge, J.-L., Pison, I., Siour, G., Turquety, S., Valari, M., Vautard, R., and
483 Vivanco, M. G.: CHIMERE 2013: a model for regional atmospheric composition modelling, *Geosci. Model Dev.*,
484 6, 981–1028, <https://doi.org/10.5194/gmd-6-981-2013>, 2013.
- 485 Menut, L., B. Bessagnet, R. Briant, A. Cholakian, F. Couvidat, S. Mailler, R. Pennel, G. Siour, P. Tuccella, S.
486 Turquety, and M. Valari. 2021. ‘The CHIMERE v2020r1 online chemistry-transport model’, *Geosci. Model Dev.*,
487 14: 6781-811.
- 488 Miyazaki, K., Eskes, H., Sudo, K., Boersma, K. F., Bowman, K., and Kanaya, Y.: Decadal changes in global surface
489 NOx emissions from multi-constituent satellite data assimilation, *Atmos. Chem. Phys.*, 17, 807-837,
490 doi:10.5194/acp-17-807-2017, 2017.
- 491 Mijling, B. and R.J. van der A, Using daily satellite observations to estimate emissions of short-lived air
492 pollutants on a mesoscopic scale, *J. Geophys. Res.*, 117, 2012, doi:10.1029/2012JD017817
- 493 Mijling et al., in preparation, 2024
- 494 Pinterits, M., B. Ullrich, T. Bartmann and M. Gager, European Union emission inventory report 1990-2019
495 under the UNECE Convention on Long-range Transboundary Air Pollution (Air Convention), EEA Report No
496 5/2021, 2021NEC, Air pollution in Europe: 2023 reporting status under the National Emission reduction
497 Commitments Directive, 2023 ([https://www.eea.europa.eu/publications/national-emission-reduction-](https://www.eea.europa.eu/publications/national-emission-reduction-commitments-directive-2023/air-pollution-in-europe-2023)
498 [commitments-directive-2023/air-pollution-in-europe-2023](https://www.eea.europa.eu/publications/national-emission-reduction-commitments-directive-2023/air-pollution-in-europe-2023))
- 499 Quitzow, R., G. Bersalli, L. Eicke, J. Jahn, J. Lilliestam, F. Lira, A. Marian, D. Süsner, S. Thapar, S. Weko, S. Williams,
500 B. Xue, The COVID-19 crisis deepens the gulf between leaders and laggards in the global energy transition,
501 *Energy Research & Social Science*, Vol. 74, 2021, 101981, <https://doi.org/10.1016/j.erss.2021.101981>.
- 502 Rijdsdijk, P., H.J. Eskes, A. Dingmans, K.F. Boersma, T. Sekiya, K. Miyazaki, and S. Houweling, Constructing
503 superobservations from satellite NO2 for assimilation and model evaluation, preprint 2024.



- 504 Sekiya, T., Miyazaki, K., Eskes, H., Sudo, K., Takigawa, M., and Kanaya, Y.: A comparison of the impact of
505 TROPOMI and OMI tropospheric NO₂ on global chemical data assimilation, *Atmos. Meas. Tech.*, 15, 1703–
506 1728, <https://doi.org/10.5194/amt-15-1703-2022>, 2022.
- 507 Shindell, D. T., Faluvegi, G., Bell, N., and Schmidt, G. A. (2005), An emissions-based view of climate forcing by
508 methane and tropospheric ozone, *Geophys. Res. Lett.*, 32, L04803, doi:[10.1029/2004GL021900](https://doi.org/10.1029/2004GL021900)
- 509 Skoulidou, I.; Koukoulis, M.-E.; Segers, A.; Manders, A.; Balis, D.; Stavrakou, T.; van Geffen, J.; Eskes, H. Changes
510 in Power Plant NO_x Emissions over Northwest Greece Using a Data Assimilation Technique. *Atmosphere* 2021,
511 12, 900. <https://doi.org/10.3390/atmos12070900>
- 512 Streets, D.G., Canty T., Carmichael, G.R., de Foy B., Dickerson, R.R. Duncan, B.N., Edwards, D.P., Haynes, J.A.,
513 Henze, D.K., Houyoux, M.R., Jacob, D.J., Krotkov, N.A., Lamsal, L.N., Liu, Y., Lu, Z., Martin, R.V., Pfister G.G.,
514 Pinder R.W., Salawitch R.J., Wecht, K.J., Emissions estimation from satellite retrievals: A review of current
515 capability, *Atmospheric Environment*, 77, 2013, 1011-1042, <https://doi.org/10.1016/j.atmosenv.2013.05.051>.
- 516 Thunis, P., M. Crippa, C. Cuvelier, D. Guizzardi, A. de Meij, G. Oreggioni, E. Pisoni, Sensitivity of air quality
517 modelling to different emission inventories: A case study over Europe, *Atmospheric Environment: X*, Volume
518 10, 2021, <https://doi.org/10.1016/j.aeaoa.2021.100111>.
- 519 van der A, R.J., de Laat, A.T.J., Ding, J., Eskes, H.J., Connecting the dots: NO_x emissions along a West Siberian
520 natural gas pipeline, *npj Clim Atmos Sci* 3, 16, <https://doi.org/10.1038/s41612-020-0119-z>, 2020
- 521 van Geffen, J. H. G. M., Eskes, H. J., Compornolle, S., Pinardi, G., Verhoelst, T., Lambert, J.-C., Sneep, M., ter
522 Linden, M., Ludewig, A., Boersma, K.F. and Veefkind, J.P.: Sentinel-5P TROPOMI NO₂ retrieval: impact of version
523 v2.2 improvements and comparisons with OMI and ground-based data, *Atmos. Meas. Tech.*, 15, 2037-2060.
524 <https://doi.org/10.5194/amt15-2037-2022>, 2022a.
- 525 van Geffen, J. H. G. M., Eskes, H. J., Boersma, K. F. and Veefkind, J. P.: TROPOMI ATBD of the total and
526 tropospheric NO₂ data products, Report S5P-KNMI-L2-0005-RP, version 2.4.0, 202207-11, KNMI, De Bilt, The
527 Netherlands, <http://www.tropomi.eu/data-products/nitrogen-dioxide/> (last access: 06 Dec. 2022), 2022b
- 528 Veefkind, J.P., Aben, I., McMullan, K., Förster, H., Vries, J., de Otter, G., Claas, J., Eskes, H.J., Haan, J.F. de,
529 Kleipool, Q., Weele, M. van, Hasekamp, O., Hoogeveen, R., Landgraf, J., Snel, R., Tol, P., Ingmann, P., Voors, R.,
530 Kruizinga, B., Vink, R., Visser, H., Levelt, P.F., 2012. TROPOMI on the ESA Sentinel-5 Precursor: a GMES mission
531 for global observations of the atmospheric composition for climate, air quality and ozone layer applications.
532 *Rem. Sens. Environ.* 120, 70–83. <https://doi.org/10.1016/j.rse.2011.09.027>.
- 533 Zhang, X., van der A, R., Ding, J., Zhang, X., and Yin, Y., Significant contribution of inland ships to the total NO_x
534 emissions along the Yangtze River, *Atmos. Chem. Phys.*, 23, 5587–5604, [https://doi.org/10.5194/acp-23-5587-](https://doi.org/10.5194/acp-23-5587-2023)
535 2023, 2023.
- 536
- 537